

F. Pei, L. Xiang, and A. Klein, "Joint Optimization of Beamforming and 3D Array-Steering for UAV-Aided ISAC", in *IEEE International Conference on Communications (ICC)*, Denver, CO, USA, June 2024.

©2024 IEEE. Personal use of this material is permitted. However, permission to reprint/republish this material for advertising or promotional purposes or for creating new collective works for resale or redistribution to servers or lists, or to reuse any copyrighted component of this works must be obtained from the IEEE.

Joint Optimization of Beamforming and 3D Array-Steering for UAV-Aided ISAC

Fengcheng Pei, Lin Xiang, and Anja Klein

Communications Engineering Lab, Technical University of Darmstadt, Germany

Email: {f.pei, l.xiang, a.klein}@nt.tu-darmstadt.de

Abstract—In this paper, we investigate unmanned aerial vehicle (UAV)-aided integrated sensing and communication (ISAC) by employing a uniform linear array (ULA) of patch antennas onboard the UAV. The three-dimensional (3D) directional gain pattern of the patch antennas and the array beamforming are jointly exploited to facilitate efficient ISAC signal transmission for sensing multiple targets and communicating with multiple users. Assuming the positions of the targets and users are known, we jointly optimize the beamforming and 3D array-steering of the patch antenna array to maximize the sum of transmit beam-pattern gains towards the targets while guaranteeing quality-of-service (QoS) for each communication user. The formulated optimization problem is nonconvex and generally intractable. Exploiting the special structures underlying the problem, we propose a low-complexity iterative algorithm based on proximal block coordinate descent (BCD) to decompose the problem into several convex and manifold optimization subproblems and iteratively solve them. Simulation results verify the benefits of joint beamforming and 3D steering optimization for UAV-aided ISAC using patch antenna array, particularly when the communication QoS requirements are stringent.

I. INTRODUCTION

Unmanned aerial vehicles (UAVs) are increasingly used in sensing and communication applications due to their agile mobility and flexible, low-cost deployment [1]. Recently, UAV-aided integrated sensing and communication (ISAC) has been proposed as a promising approach to realize efficient simultaneous wireless sensing and communication onboard UAVs. ISAC enables a light-weight design ideal for UAVs constrained by size, weight, and power (SWAP), as it allows for onboard sensing and communication using shared spectrum, signal processing algorithms, and transmitter hardware [2]. Moreover, by employing a common signal for sensing and communication, rather than separate, potentially interfering signals, ISAC enhances the utilization of limited radio resources [3]. Further, mobile UAVs can also improve the ISAC performance by e.g. proactively seeking strong line-of-sight (LoS) channels and avoiding obstacles between the UAV and sensing targets or communication users [4], especially in emergency scenarios or complex environments [5].

The appealing synergies between UAVs and ISAC have motivated several recent works to explore joint design and optimization of UAV's movements and ISAC signal transmission for UAV-aided ISAC [6]–[12]. In [6]–[8], the authors equipped the UAV with a uniform linear array (ULA) and jointly optimized the transmit beamforming and flight trajectory of the UAV for maximizing the system throughput while ensuring quality-of-service (QoS) for sensing. In [9] and [10], energy efficiency maximization for UAV-aided ISAC was investigated. However, the isotropic antennas assumed in [6]–[10] are generally ideal and ignore the three-dimensional (3D) directional radiation pattern of real-world antennas. In [11], UAV-assisted

networks employing arrays of directional antennas were considered, where the authors investigated the optimal antenna directivity factor for balancing between sensing coverage and network connectivity. Moreover, the authors of [12] evaluated the impact of vertical and horizontal placements of a dipole antenna array for UAV-aided localization. Note that fixed antenna array orientations were assumed in both [11] and [12].

The aforementioned works [6]–[12] revealed a fundamental performance trade-off between sensing and communication for UAV-aided ISAC, depending on the signal power radiated towards the sensing targets and the communication users. With an array of directional antennas, the radiation pattern for ISAC signal transmission can be spatially shaped either via beamforming or by antenna/array steering [13]. This raises an interesting open research question, i.e., *how to jointly exploit both techniques to best trade-off between sensing and communication performance for UAV-aided ISAC* [14]. Note that the fixed array steering in [11], [12] is not optimal, as the resulting antenna element radiation pattern may be misaligned with the array/beam pattern. For example, sensing targets or communication users lying outside the peak radiation direction of directional antennas have to be illuminated by beamforming, but using lower gains of the directional antennas.

This paper aims to address the above research question by exploiting a novel synergy between UAV and ISAC for UAV-aided ISAC. In particular, unlike [6]–[12], we exploit the UAV's movement or an onboard gimbal for rotating (rather than translating) the array in the 3D space. Also, unlike [11], [12], the UAV employs a ULA of patch antennas with half-wavelength size, which are widely used in practical communications. As such, the 3D directional radiation pattern of patch antennas and the array orientation can be utilized together with beamforming to shape highly-directive beams desired for e.g. radar sensing and to better trade-off between sensing and communication than [6]–[12].

To reap the performance gains of the proposed approach, we further jointly optimize the beamforming and 3D array-steering for maximizing the total power radiated towards multiple sensing targets while guaranteeing QoS for multiple communication users. Due to the 3D array-steering, the formulated optimization problem is highly nonconvex and becomes much more difficult to solve than the ones in [6]–[12]. To facilitate a low-complexity solution, we decompose the problem into multiple convex and manifold optimization subproblems, which are further solved using an iterative algorithm. Our contributions are :

- We consider joint beamforming and 3D steering of a ULA with patch antennas to enable efficient signal transmission for UAV-aided ISAC. We formulate a highly nonconvex problem for maximizing the sum of transmit beam-pattern gains towards the targets while guaranteeing QoS requirements for each communication user.
- Exploiting the underlying problem structure, we further propose a low-complexity iterative algorithm based on the

This work has been funded by the LOEWE initiative (Hesse, Germany) within the emergenCITY center and has been supported by the BMBF project Open6GHub under grant 16KISKO14 and by DAAD with funds from the German Federal Ministry of Education and Research (BMBF).

proximal block coordinate descent (BCD) together with convex and manifold optimization techniques to solve the problem.

- Simulation results show that joint beamforming and 3D steering of patch antenna array significantly outperforms isotropic antenna array in expanding the achievable sensing and communication performance region due to its high directivity and the additional degrees of freedom (DoF) of rotation, even with a small number of antennas.

In the remainder of this paper, Section II introduces the system model. The problem formulation and the proposed solution are provided in Sections III and IV, respectively. Section V presents the simulation results and finally, Section VI concludes the paper.

Notation: Throughout this paper, matrices and vectors are denoted by boldface capital and lower-case letters, respectively. $\mathbb{C}^{m \times n}$ and $\mathbb{R}^{m \times n}$ denote $m \times n$ complex- and real-valued matrices, respectively. $j = \sqrt{-1}$ is the imaginary unit of a complex number and $\|\cdot\|$ is the l_2 -norm of a vector. \mathbf{A}^T and \mathbf{A}^H are the transpose and complex conjugate transpose of matrix \mathbf{A} , respectively. $\text{tr}(\mathbf{A})$ and $\text{rank}(\mathbf{A})$ denote the trace and rank of matrix \mathbf{A} , respectively. Finally, $\vec{\mathbf{A}}$ and $\vec{\mathbf{a}}$ denote a displacement vector and its unit direction vector, respectively, which satisfy $\vec{\mathbf{a}}_k = \vec{\mathbf{A}}_k / \|\vec{\mathbf{A}}_k\|$.

II. SYSTEM MODEL

We consider a UAV-aided ISAC system as shown in Fig. 1. A rotary-wing UAV acts as a dual-functional aerial access point (AP) to perform downlink communication with multiple ground/aerial users and radar sensing towards multiple targets simultaneously. Let $\mathcal{K} = \{1, \dots, K\}$ and $\mathcal{L} = \{1, \dots, L\}$ be the sets of communication users and sensing targets, respectively. We assume that the UAV hovers at a given position $P(x, y, H)$. Meanwhile, the positions of user $k \in \mathcal{K}$ and target $l \in \mathcal{L}$, denoted by $U_k(x_k, y_k, z_k)$ and $T_l(x_l, y_l, z_l)$, respectively, are fixed. To enhance both sensing and communication, we equip the UAV with a transmit ULA of N patch antennas, each with dimensions half the carrier wavelength in both length and width. Since we focus on ISAC signal transmission, we assume that each communication user has a single receive antenna.

A. 3D Channel Model for UAV-aided ISAC

We assume that a strong LoS link typically exists between the elevated UAV and each user or target [8]. The channel vector between the UAV and user $k \in \mathcal{K}$ is modeled as

$$\mathbf{h}_k = \frac{\sqrt{\beta}}{\|\vec{\mathbf{D}}_k\|} \cdot \mathbf{a}_{U,k}, \quad (1)$$

where β denotes the channel power gain at unit distance. $\vec{\mathbf{D}}_k = (x_k - x, y_k - y, z_k - H)^T$ and its norm, $\|\vec{\mathbf{D}}_k\|$, capture the displacement vector and the distance between the UAV and user k , respectively. Finally, $\mathbf{a}_{U,k} \in \mathbb{C}^{N \times 1}$ denotes the array steering vector for user k .

It remains to characterize the array steering vector $\mathbf{a}_{U,k}$ for the ULA with patch antennas. To this end, we define orthogonal unit vectors $\vec{\mathbf{r}}_a \in \mathbb{R}^{3 \times 1}$ and $\vec{\mathbf{r}}_p \in \mathbb{R}^{3 \times 1}$ to denote the direction of array axis and its orthogonal direction within the array plane, respectively, as illustrated in Fig. 2. We have $\vec{\mathbf{r}}_a^T \cdot \vec{\mathbf{r}}_p = 0$. The unit vectors $\vec{\mathbf{r}}_a$ and $\vec{\mathbf{r}}_p$ uniquely determine the spatial orientation of the patch antenna array during 3D rotation. Meanwhile, they can enable a convenient modeling of

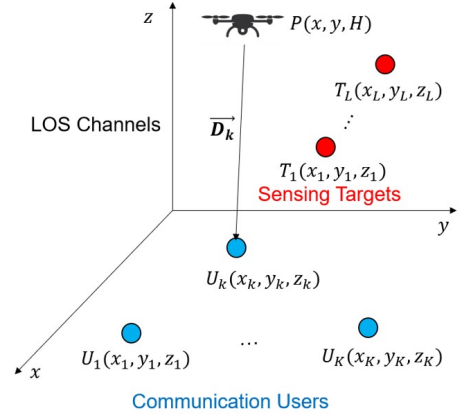


Fig. 1. System model of UAV-aided ISAC.

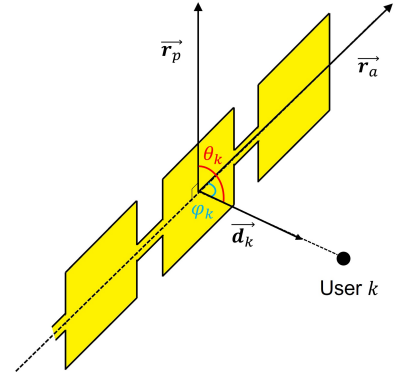


Fig. 2. Transmit ULA with patch antennas deployed at the UAV.

the 3D radiation characteristics. For the latter purpose, let φ_k be the angle formed by unit direction vectors $\vec{\mathbf{d}}_k \triangleq \vec{\mathbf{D}}_k / \|\vec{\mathbf{D}}_k\|$ and $\vec{\mathbf{r}}_a$. Similarly, let θ_k denote the angle between $\vec{\mathbf{d}}_k$ and $\vec{\mathbf{r}}_p$. For convenience, we refer to θ_k and φ_k as the elevation and azimuth angles for user k (relative to $\vec{\mathbf{r}}_p$ and $\vec{\mathbf{r}}_a$), respectively. We have

$$\varphi_k = \arccos(\vec{\mathbf{d}}_k^T \cdot \vec{\mathbf{r}}_a) \quad (2)$$

$$\theta_k = \arccos(\vec{\mathbf{d}}_k^T \cdot \vec{\mathbf{r}}_p), \quad (3)$$

which are only functions of $\vec{\mathbf{r}}_a$ and $\vec{\mathbf{r}}_p$ for given $\vec{\mathbf{d}}_k$.

Finally, the steering vector $\mathbf{a}_{U,k}$ is modeled as [16]

$$\mathbf{a}_{U,k} = \alpha \cdot \text{EF}(\varphi_k, \theta_k) \cdot \text{AF}(\varphi_k), \quad (4)$$

where $\text{EF}(\varphi_k, \theta_k)$ and $\text{AF}(\varphi_k)$ denote the element factor and array factor, respectively, and α is a normalization coefficient to limit the total power radiated into the space with $\frac{1}{4\pi^2} \int_0^\pi \int_0^\pi \text{EF}(\varphi_k, \theta_k) = 1$. We assume that all users are located in the far-field of the array and the patch antennas work in the fundamental resonance mode [16]. According to the antenna theory [16], the element factor $\text{EF}(\varphi_k, \theta_k)$ in (4) can be approximated as

$$\text{EF}(\varphi_k, \theta_k) = \sin(\varphi_k) \cdot \sin(\theta_k), \quad (5)$$

and the array factor $\text{AF}(\varphi_k)$ is given by

$$\text{AF}(\varphi_k) = (1, e^{j\frac{2\pi}{\lambda}d \cdot \cos \varphi_k}, \dots, e^{j(N-1)\frac{2\pi}{\lambda}d \cdot \cos \varphi_k})^T, \quad (6)$$

where λ and d denote the carrier wavelength and the spacing

between adjacent patch antennas in the array, respectively.

$$\text{C5: SINR}_k \geq r_k, k \in \mathcal{K}. \quad (\text{P1})$$

B. Signal Model and Radiation Gain Pattern

The transmitted signal of the UAV is given by

$$\mathbf{s} = \sum_{k=1}^K \mathbf{w}_k \cdot s_k, \quad (7)$$

where $s_k \in \mathbb{C}$ denotes the data symbol intended for user $k \in \mathcal{K}$. We assume that s_k follows the circularly symmetric complex Gaussian (CSCG) distribution with zero mean and unit variance, i.e., $s_k \sim \mathcal{CN}(0, 1)$. $\mathbf{w}_k \in \mathbb{C}^{N \times 1}$ is the beamforming vector associated with s_k . Meanwhile, the received signal at user k is given as

$$y_k = \mathbf{h}_k^H \sum_{k=1}^K \mathbf{w}_k \cdot s_k + n_k, \quad (8)$$

where $n_k \in \mathbb{C}$ denotes the noise received at user k and is modeled as a zero-mean CSCG random variable with variance σ_k^2 , i.e., $n_k \sim \mathcal{CN}(0, \sigma_k^2)$. As a result, the achievable data rate of user k in bps/Hz is

$$R_k = \log_2(1 + \text{SINR}_k), \quad (9)$$

$$\text{SINR}_k = \frac{|\mathbf{h}_k^H \mathbf{w}_k|^2}{\sum_{m=1, m \neq k}^K |\mathbf{h}_k^H \mathbf{w}_m|^2 + \sigma_k^2}, \quad (10)$$

where SINR_k denotes the received signal-to-interference-plus-noise ratio (SINR) of user k . Moreover, the transmit beam pattern gain towards target $l \in \mathcal{L}$ is given by [15]

$$P_{T,l} = \sum_{k=1}^K |\mathbf{w}_k^H \mathbf{a}_{T,l}|^2, \quad (11)$$

where $\mathbf{a}_{T,l}$ is the steering vector of the transmit patch antenna array toward target l . Note that $\mathbf{a}_{T,l}$ can be calculated by replacing the angle pairs (φ_k, θ_k) in (4) with (φ_l, θ_l) .

For sensing purposes, a monostatic radar receiver onboard the UAV or another bistatic radar receiver needs to detect and process echoes of the communication signal reflected/scattered by the targets to realize action recognition and, when necessary, distinguish different targets using features extracted from the echoes, including round-trip time, angle of arrival, and received power, etc. However, its detailed modeling is ignored in this paper.

III. PROBLEM FORMULATION

The achievable data rate R_k of user k and the transmit beam pattern gain $P_{T,l}$ towards target l in (9) and (11) depend on both the beamforming vector, \mathbf{w}_k , and the orientation/steering of the patch antenna array, $\{\bar{\mathbf{r}}_a, \bar{\mathbf{r}}_p\}$. Hence, joint optimization of beamforming and array steering is crucial to maximize the performance of the considered UAV-aided ISAC system, which is investigated in this section. Our goal is to maximize the radiated sensing power, measured by the sum of transmit beam pattern gains towards all the targets while guaranteeing QoS for each communication user. The resulting optimization problem is formulated as

$$\begin{aligned} & \underset{\mathbf{w}_k, \bar{\mathbf{r}}_a, \bar{\mathbf{r}}_p}{\text{maximize}} && \sum_{l=1}^L P_{T,l} \\ & \text{subject to} && \text{C1: } \|\mathbf{w}_k\|^2 \leq P_k, k \in \mathcal{K} \\ & && \text{C2: } \|\bar{\mathbf{r}}_a\| = 1, \\ & && \text{C3: } \|\bar{\mathbf{r}}_p\| = 1 \\ & && \text{C4: } \bar{\mathbf{r}}_a \cdot \bar{\mathbf{r}}_p = 0 \end{aligned}$$

In (P1), constraint C1 limits the maximal transmit power allocated for user k by P_k , where $\sum_{k=1}^K P_k = P_{\max}$ and P_{\max} is the total transmit power of the UAV. We assume that P_k is given a priori in this paper, but since it is an affine term, it can also be optimized using our proposed solution. Constraints C2, C3 and C4 indicate that $\bar{\mathbf{r}}_a$ and $\bar{\mathbf{r}}_p$ are unit vectors being orthogonal to each other, cf. Fig. 2. Finally, C5 guarantees a minimum received SINR of r_k , or equivalently a minimum data rate of $\log_2(1 + r_k)$ in bps/Hz, for each communication user k to meet the QoS requirement.

Problem (P1) is nonconvex due to the nonconvex constraints C2, C3, C4, and C5, hindering its optimal solution. Moreover, the optimization of beamforming vectors \mathbf{w}_k and array steering vectors $\{\bar{\mathbf{r}}_a, \bar{\mathbf{r}}_p\}$ are tightly coupled with each other due to the objective function and constraint C5. This type of problem is generally NP-hard. It can be solved optimally by algorithms with exponential-time complexity. But algorithms that can optimally solve it in polynomial time are not known yet [17]. In order to facilitate real-time resource allocation for UAV-aided ISAC, in Sec. IV, we propose a polynomial-time suboptimal solution for (P1) by exploiting its underlying problem structures.

IV. PROBLEM SOLUTION

As will be shown in this section, the beamforming optimization in problem (P1) exhibits a hidden convexity. Meanwhile, the constraints C2, C3, and C4 define a special manifold structure. Exploiting both problem structures, we present in this section an iterative proximal BCD algorithm [18], which decomposes problem (P1) into several subproblems and solve them iteratively using convex and manifold optimization techniques. The subproblems optimize each of the three variable blocks in (P1), namely $\{\mathbf{w}_k\}$, $\{\bar{\mathbf{r}}_a\}$, and $\{\bar{\mathbf{r}}_p\}$, while keeping the other two blocks of variables fixed. To decouple the optimization of beamforming and steering and to guarantee convergence of the iterations, we introduce penalty and proximal terms into the objective function of the subproblems of (P1), respectively. We then discuss the solution of each subproblem.

A. Beamforming Optimization Exploiting Hidden Convexity

For given array orientation $\{\bar{\mathbf{r}}_a, \bar{\mathbf{r}}_p\}$, the subproblem for optimizing the beamforming vector $\{\mathbf{w}_k\}$ is defined as

$$\begin{aligned} & \underset{\mathbf{w}_k \in \mathbb{C}^{N \times 1}}{\text{maximize}} && \sum_{l=1}^L P_{T,l} \\ & \text{subject to} && \text{C1, } \bar{\text{C5}}: \sum_{m=1, m \neq k}^K r_k \cdot |\mathbf{h}_k^H \mathbf{w}_m|^2 \\ & && - |\mathbf{h}_k^H \mathbf{w}_k|^2 + r_k \cdot \sigma_k^2 \leq 0, k \in \mathcal{K}. \end{aligned} \quad (\text{P2})$$

Note that in (P2), we have rewritten C5 as $\bar{\text{C5}}$ in a quadratic form. As a result, (P2) is a quadratically constrained quadratic program (QCQP). To solve (P2), let $\mathbf{V}_k = \mathbf{w}_k \mathbf{w}_k^H$, i.e., $\mathbf{V}_k \in \mathbb{C}^{N \times N}$ is a symmetric and positive semidefinite matrix with rank one. Using \mathbf{V}_k , (P2) is equivalently reformulated as

$$\begin{aligned} & \underset{\mathbf{V}_k \in \mathbb{C}^{N \times N}}{\text{maximize}} && \sum_{l=1}^L \sum_{k=1}^K \text{tr}(\mathbf{A}_{T,l} \mathbf{V}_k) \\ & \text{subject to} && \bar{\text{C1}}: \text{tr}(\mathbf{V}_k) \leq P_k, k \in \mathcal{K} \\ & && \bar{\text{C5}}: \sum_{m \neq k} r_k \cdot \text{tr}(\mathbf{H}_k \mathbf{V}_m) - \text{tr}(\mathbf{H}_k \mathbf{V}_k) + r_k \sigma_k^2 \leq 0 \end{aligned}$$

Algorithm 1 REPMS for solving problem (P5)

Input: Initial $\gamma_{a,0}^*$, initial penalty weight ρ_0 , initial smoothing factor u_0 , $\delta_\rho > 1$, $0 < \delta_u < 1$, u_{\min} , ρ_{\max} , stopping threshold ϵ , $q_0 = \|\gamma_{a,0}\|$ and $t = 0$

Output: Optimal γ_a^*

- 1: **while** $q_t > \epsilon$ **do**
 - 2: Optimize problem (P5) with $\rho = \rho_t$ and $u = u_t$ by RCG manifold optimization, and get $\gamma_{a,t+1}^*$.
 - 3: $\rho_{t+1} = \min\{\delta_\rho \rho_t, \rho_{\max}\}$.
 - 4: $u_{t+1} = \max\{\delta_u u_t, u_{\min}\}$.
 - 5: $q_{t+1} = \|\gamma_{a,t+1}^* - \gamma_{a,t}^*\|$.
 - 6: $t = t + 1$.
 - 7: **end while**
-

$$\text{C6: } \mathbf{V}_k \succeq \mathbf{0}, \text{ C7: } \text{rank}(\mathbf{V}_k) = 1, k \in \mathcal{K}, \quad (\text{P3})$$

with $\mathbf{A}_{T,l} \triangleq \mathbf{a}_{T,l} \mathbf{a}_{T,l}^H$ and $\mathbf{H}_k \triangleq \mathbf{h}_k \mathbf{h}_k^H$.

Problem (P3) is still NP-hard, because of the rank constraint C7. However, by dropping or relaxing C7, the resulting problem become a convex SDP, given as

$$\begin{aligned} & \underset{\mathbf{V}_k \in \mathbb{C}^{N \times N}}{\text{maximize}} && \sum_{l=1}^L \sum_{k=1}^K \text{tr}(\mathbf{A}_{T,l} \mathbf{V}_k) \\ & \text{subject to} && \overline{\text{C1}}, \overline{\text{C5}}, \text{C6.} \end{aligned} \quad (\overline{\text{P3}})$$

(P3) can be then tackled using either iterative dual gradient descent method or available solvers such as CVX [17]. In general, the solution of the relaxed problem (P3), denoted by \mathbf{V}_k^* , may have a rank other than one, i.e., $\text{rank}(\mathbf{V}_k^*) \neq 1$. In this case, the optimal value of (P3) only serves an upper bound for that of (P3). However, we show below that this is not the case, because problem (P3) has a *hidden convexity* in the sense that (P3) is equivalent to the convex problem (P3).

Lemma 1: Assume that problem (P3) admits at least one feasible solution. Then we can always obtain an optimal rank-one solution \mathbf{V}_k^* by solving the relaxed SDP problem of (P3), i.e., the SDP relaxation is tight.

Proof: Due to limited page space, the details are ignored. Please refer to [20, Theorem 2] for a similar proof. The Lemma has also been validated offline using simulations. ■

B. Array Steering Using Manifold Optimization

We now optimize the array orientation $\{\vec{\mathbf{r}}_a, \vec{\mathbf{r}}_p\}$ for given beamforming vectors $\{\mathbf{w}_k\}$. In the subsequent discussion, we only elaborate the solution for optimizing $\{\vec{\mathbf{r}}_a\}$. By utilizing the symmetry between $\{\vec{\mathbf{r}}_a\}$ and $\{\vec{\mathbf{r}}_p\}$, the solution for optimizing $\{\vec{\mathbf{r}}_p\}$ can be obtained by interchanging $\{\vec{\mathbf{r}}_a\}$ and $\{\vec{\mathbf{r}}_p\}$ in the proposed method. The subproblem of optimizing $\{\vec{\mathbf{r}}_a\}$ is formulated as

$$\begin{aligned} & \underset{\vec{\mathbf{r}}_a \in \mathbb{R}^{3 \times 1}}{\text{maximize}} && \sum_{l=1}^L P_{T,l} - c \cdot \|\vec{\mathbf{r}}_a - \vec{\mathbf{r}}_a'\|^2 \\ & && - \rho \cdot \sum_{k=1}^K \max\{0, r_k - \text{SINR}_k\} \\ & \text{subject to} && \text{C2, C4,} \end{aligned} \quad (\text{P4})$$

where $c \geq 0$ and $\rho > 0$ are penalty factors. $\vec{\mathbf{r}}_a'$ is the direction vector obtained in the last iteration. The quadratic proximal term $c \cdot \|\vec{\mathbf{r}}_a - \vec{\mathbf{r}}_a'\|^2$ is employed to enhance convergence of

Algorithm 2 Proposed proximal BCD algorithm to solve (P1)

Input: $\mathbf{W}_0 = [\mathbf{w}_{1,0}, \dots, \mathbf{w}_{K,0}]$, $\vec{\mathbf{r}}_{a,0}$, $\vec{\mathbf{r}}_{p,0}$ and $i = 1$

Output: Optimal $\mathbf{W}^* = [\mathbf{w}_1^*, \dots, \mathbf{w}_K^*]$, $\vec{\mathbf{r}}_a^*$ and $\vec{\mathbf{r}}_p^*$

- 1: **Repeat**
 - 2: Solve (P2) for $\vec{\mathbf{r}}_p = \vec{\mathbf{r}}_{p,i-1}$ and $\vec{\mathbf{r}}_a = \vec{\mathbf{r}}_{a,i-1}$ with SDP relaxation, and set $\mathbf{W}_i = \mathbf{W}^*$.
 - 3: Find an orthonormal basis \mathbf{v} in the null space of $\vec{\mathbf{r}}_p = \vec{\mathbf{r}}_{p,i-1}$.
 - 4: Optimize γ_a in (P5) with Algorithm 1 for $\mathbf{W} = \mathbf{W}_i$ and $\vec{\mathbf{r}}_p = \vec{\mathbf{r}}_{p,i-1}$.
 - 5: Calculate $\vec{\mathbf{r}}_a^*$ with (12) and set $\vec{\mathbf{r}}_{a,i} = \vec{\mathbf{r}}_a^*$.
 - 6: Optimize $\vec{\mathbf{r}}_p$ for $\mathbf{W} = \mathbf{W}_i$ and $\vec{\mathbf{r}}_a = \vec{\mathbf{r}}_{a,i}$, similar to Step 3, 4 and 5, and set $\vec{\mathbf{r}}_{p,i} = \vec{\mathbf{r}}_p^*$.
 - 7: $i = i + 1$.
 - 8: **Until** Convergence
-

the iterations, by convexifying problem (P4) and penalizing large deviations between the optimal solution of (P4) and $\vec{\mathbf{r}}_a'$. The last term in the objective function is a weighted exact penalty for preventing violations of constraint C5 [21].

By introducing the exact penalty term in (P4), the remaining constraints C2 and C4 define a smooth manifold, i.e., a unit circle, given by the intersection of a unit sphere defined by C2 and a plane defined by C4. Such manifold constraint can be conveniently tackled with manifold optimization. However, the non-differentiable/non-smooth $\max\{\cdot, \cdot\}$ function in the objective function is difficult to handle in a straightforward manner by manifold optimization. Here, we further approximate the $\max\{\cdot, \cdot\}$ function using a smooth log-sum-exp function [21]. The smoothed optimization problem is given as

$$\begin{aligned} & \underset{\vec{\mathbf{r}}_a \in \mathbb{R}^{3 \times 1}}{\text{minimize}} && - \sum_{l=1}^L P_{T,l} + c \cdot \|\vec{\mathbf{r}}_a - \vec{\mathbf{r}}_a'\|^2 \\ & && + \rho \cdot \sum_{k=1}^K u \log(1 + e^{\frac{r_k - \text{SINR}_k}{u}}) \\ & \text{subject to} && \text{C2, C4,} \end{aligned} \quad (\text{P5})$$

where $u > 0$ is the smoothing factor. Note that we have transformed (P4) into a minimization problem in (P5) by changing the sign in the objective function.

Problem (P5) can now be solved by the Riemannian conjugate gradient (RCG) method, which is an extension of conjugate gradient descent method on Riemannian manifolds [23]. To this end, we first transform C2 and C4 into a manifold constraint. For convenience, we denote the objective function of (P5) by $f(\vec{\mathbf{r}}_a)$. Let $\vec{\mathbf{r}}_p'$ be the optimal direction obtained in the last iteration. Assume that \mathbf{v}_i , $i = 1, 2$ are the orthonormal bases for the null space of $\vec{\mathbf{r}}_p'$. We substitute the optimization variable $\vec{\mathbf{r}}_a$ in (P5) by

$$\vec{\mathbf{r}}_a = \mathbf{v} \cdot \gamma_a, \quad (12)$$

where $\mathbf{v} = [\mathbf{v}_1, \mathbf{v}_2] \in \mathbb{R}^{3 \times 2}$ and $\gamma_a \in \mathbb{R}^{2 \times 1}$ is the new optimization variable with $\|\gamma_a\| = 1$. As a result, problem (P5) is reformulated as

$$\underset{\gamma_a \in \mathbb{R}^{2 \times 1}}{\text{minimize}} \quad f(\mathbf{v} \cdot \gamma_a) \quad (\overline{\text{P5}})$$

$$\text{subject to} \quad \text{C8: } \|\gamma_a\| = 1,$$

where C8 defines a unit-circle manifold. Problem (P5) is then

solved with off-the-shelf solvers such as pymanopt [23].

The overall procedure for solving (P5), known as the Riemannian exact penalty method via smoothing (REPMS), is summarized in Algorithm 1. The value of penalty factor ρ should be chosen carefully, because an extremely large ρ may slow down the convergence and even lead to an ill-conditioning problem. Hence, in Algorithm 1, we start with setting a relatively small initial value for ρ . We then iteratively increase ρ and optimize γ_a in (P5) [21]. The overall algorithm for solving problem (P1) is presented in Algorithm 2.

V. SIMULATION RESULTS

In this section, we evaluate the performance of the proposed scheme for joint beamforming and array steering optimization in a UAV-aided ISAC system by simulation. As shown in Fig. 3(a), the UAV hovers at position $P(0, 0, 20)$ for communicating with $K = 2$ ground users and sensing $T = 2$ targets simultaneously. The users are located at $U_1(-110, 600, 0)$ and $U_2(110, 600, 0)$, respectively, while the targets are located in close proximity of the UAV at $T_1(6, 1, 10)$ and $T_2(-5, 4, 25)$. In Fig. 3(a), we indicate the users by colored dots, and the directions of targets via colored vectors. We assume that the UAV has LoS channels to all users and targets. The UAV employs a ULA of $N = 8$ patch antennas, spaced by $d = \lambda/2$ apart, and the carrier wavelength is $\lambda = 10$ mm. The maximal transmit power of the UAV is $P_{\max} = 2$ W and is equally shared among the communication users for fairness, i.e., $P_1 = P_2 = P_{\max}/2$. The minimum required SINR r_k is set to 1 for all users, in order to ensure a minimum data rate of $\log_2(1 + r_k) = 1$ bps/Hz per user. The upper bound of penalty factor ρ_{\max} and the lower bound of smoothing factor u_{\min} are set to 10^6 and 10^{-6} [22], respectively. Finally, the noise power and the path loss coefficient are set as $\sigma_k^2 = 10^{-12}$ W, $k \in \mathcal{K}$, and $\beta = 10^{-6}$, respectively. The array orientation is initialized as $\vec{r}_{a,0} = (1, 0, 0)^T$ and $\vec{r}_{p,0} = (0, 0, 1)^T$. Under the initial setting, the users and the targets observe significantly different azimuth angles relative to $\vec{r}_{a,0}$. To illustrate this fact, Fig. 3(a) draws colored transparent planes for the corresponding users and targets at different azimuth angles. For performance comparison, we consider the following schemes as benchmarks,

- *Baseline Scheme 1:* The UAV utilizes a ULA of isotropic elements. The array orientation and beamforming are jointly optimized using Algorithm 2.
- *Baseline Scheme 2:* The UAV utilizes a ULA of isotropic elements, with fixed array orientation $(1, 0, 0)^T$.
- *Baseline Scheme 3:* The UAV utilizes a ULA of patch antennas, with fixed array orientation $\vec{r}_a = (1, 0, 0)^T$ and $\vec{r}_p = (0, 0, 1)^T$.

For Baseline Schemes 2 and 3, beamforming is optimized using the SDP relaxation approach as in Algorithm 1.

Fig. 3(b) and Fig. 3(c) evaluate the sum of transmit beam-pattern gains towards the targets achieved with the considered schemes for different minimum data rates requested by the users and different number of transmit antennas, respectively. From Fig. 3(b) we observe that, for Baseline Schemes 1 and 2, the sum of beam-pattern gains decrease significantly with the minimum required data rate. Particularly, when the data rate exceeds 3.5 bps/Hz. This reveals an inherent trade-off between sensing performance and communication QoS. Baseline Schemes 1 and 2 even fail to satisfy the minimum required data rates beyond 4.5 bps/Hz, as the considered ISAC scenario with dispersed user and target positions is quite demanding for

ULA of isotropic elements. By optimizing the array steering, Baseline Scheme 1 achieves approximately 2.5 dBi gains over Baseline Scheme 2 in the sensing performance. This is because, by array steering, Baseline Scheme 1 can adjust the azimuth angles of the users and targets and the array factor in (6), which improves the beamforming gain of the ULA.

Fig. 3(b) also reveals that employing the ULA of patch antennas can achieve significantly higher sensing performance than the ULA of isotropic antennas. For example, even with a fixed array orientation, Baseline Scheme 3 gains more than 9 dBi over Baseline Scheme 1 for all considered communication data rates and the gain increases to 14 dBi for high data rate requirements. This is because the highly directive patch antennas can focus the signal energy to effectively illuminate the users and targets. Interestingly, optimization of array orientation is more beneficial for ULA of patch antennas than ULA of isotropic antennas. For example, the proposed scheme gains 4 dBi in sensing performance over Baseline Scheme 3. Also, the proposed scheme achieves the best performance and best trade-off between sensing and communication characterized by the largest achievable sensing and communication performance region. On the other hand, Fig. 3(c) shows that, for all considered schemes, the sensing performance further improves as number of transmit antennas increases, since more spatial DoFs can be exploited for beamforming. Interestingly, the proposed scheme already achieves significantly high performance even with a small number of antennas, highlighting its potential for applications in UAVs with SWAP constraints.

For insights into the performance gains of the proposed scheme, Fig. 4 compares the optimized transmit gain patterns of all considered schemes, where the dashed lines denote the normalized azimuth angle, φ_k/π , of each user or target relative to the UAV's array orientation vector \vec{r}_a . Figs. 4(a) and 4(b) compare the performance of beamforming using ULA of isotropic elements without and with array steering, respectively. We observe that, without array steering, Baseline Scheme 2 splits the beam toward the directions of each target. Meanwhile, due to limited spatial DoFs, the users can only communicate with low pattern gains. In contrast, Baseline Scheme 1 utilizes array steering to align both targets and user 1 into the same beam for sensing and communication. Due to the alignment, high-gain beam can also be shaped to outperform Baseline Scheme 2 in sensing.

Figs. 4(c) and 4(d) compare the performance of beamforming using ULA of patch elements without and with array steering, respectively. Unlike the ULA of isotropic elements in Figs. 4(a) and 4(b), each target or user observes a different gain pattern due to the 3D directional radiation pattern of patch antennas. Meanwhile, the ULA of patch elements can shape beams with much larger gain patterns than the ULA of isotropic elements, due to the high directivity of patch antennas. Therefore, Baseline Scheme 3 with fixed array orientation can significantly outperform Baseline Schemes 1 and 2. With array steering, the proposed scheme aligns the users and targets in both azimuth angles and elevation angles. Through further joint optimization of array steering and beamforming, the proposed scheme utilizes the available spatial DoFs to achieve the best performance.

VI. CONCLUSIONS AND FUTURE WORK

In this paper, we considered joint beamforming and 3D steering of a ULA with patch antennas for UAV-aided ISAC.

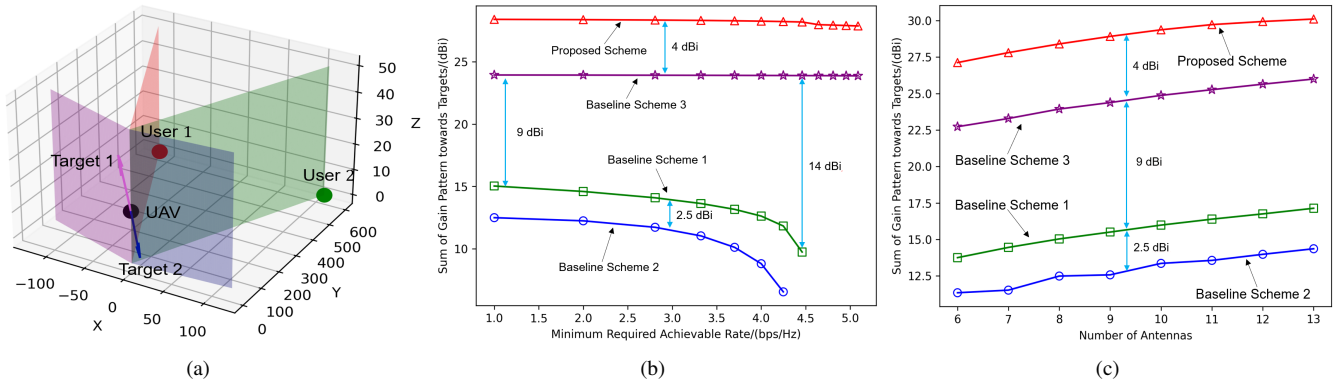


Fig. 3. (a) Initial system settings in a 3D space with dimensions 200m×600m×50m and (b)–(c) performance comparison of considered schemes for (b) increasing minimum required data rates of users and (c) increasing number of antennas.

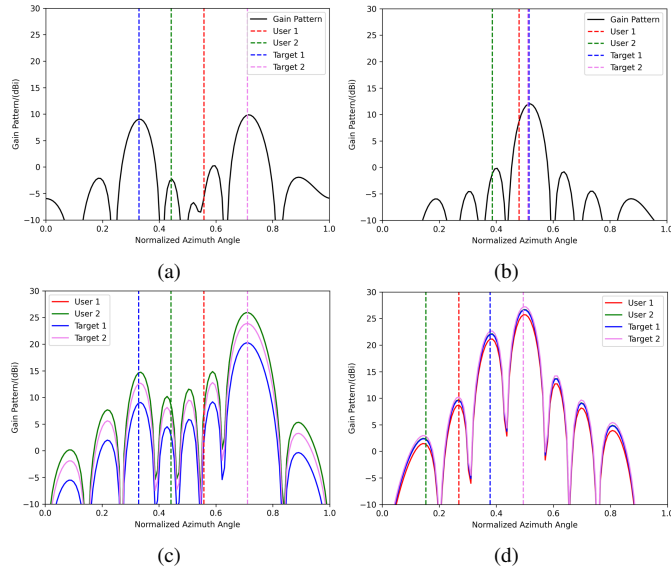


Fig. 4. Optimized array gain patterns of (a) Baseline 2, (b) Baseline 1, (c) Baseline 3, and (d) Proposed scheme.

We formulated a highly nonconvex optimization problem for maximizing the sum of transmit beam pattern gains towards the targets while guaranteeing a minimum received SINR for each communication user. Exploiting the underlying problem structures, we further propose a low-complexity iterative algorithm based on the proximal BCD together with convex and manifold optimization techniques to solve the problem. Simulation results showed that with joint optimization of beamforming and array steering, the ULA with patch antennas significantly outperforms the ULA with isotropic antennas in achieving higher beam pattern gains for sensing while satisfying more stringent communication QoS, even with a small number of patch antennas. In this paper, we have assumed that the UAV hovers at a fixed location, in order to explore the benefits of antenna array steering. Joint optimization of beamforming, array steering, and flight trajectory for UAV-aided ISAC is an interesting topic left for future research.

REFERENCES

- [1] G. Geraci, et al., “What Will the Future of UAV Cellular Communications Be? A Flight From 5G to 6G,” *IEEE Commun. Surveys & Tut.*, vol. 24, no. 3, pp. 1304-1335, 3rd quarter 2022.
- [2] J. A. Zhang et al., “Enabling Joint Communication and Radar Sensing in Mobile Networks—A Survey,” *IEEE Commun. Surveys & Tut.*, vol. 24, no. 1, pp. 306-345, 1st quarter 2022.
- [3] S. Bartoletti, N. Decarli and B. M. Masini, “Sideline 5G-V2X for Integrated Sensing and Communication: the Impact of Resource Allocation,” *2022 IEEE International Conference on Communications Workshops*, Seoul, Korea, Republic of, 2022, pp. 79-84.
- [4] M. Mozaffari, W. Saad, et al., “A Tutorial on UAVs for Wireless Networks: Applications, Challenges, and Open Problems,” *IEEE Commun. Surveys & Tut.*, vol. 21, no. 3, pp. 2334-2360, 3rd quarter 2019.
- [5] Q. Wu, Y. Zeng and R. Zhang, “Joint Trajectory and Communication Design for Multi-UAV Enabled Wireless Networks,” *IEEE Trans. Wireless Commun.*, vol. 17, no. 3, pp. 2109-2121, Mar. 2018.
- [6] K. Meng, Q. Wu, et al., “UAV Trajectory and Beamforming Optimization for Integrated Periodic Sensing and Communication,” *IEEE Wireless Commun. Lett.*, vol. 11, no. 6, pp. 1211-1215, Jun. 2022.
- [7] C. Deng, X. Fang and X. Wang, “Beamforming design and trajectory optimization for UAV-empowered adaptable integrated sensing and communication,” *IEEE Trans. Wireless Commun.* (accepted), Apr. 2023.
- [8] Z. Lyu, G. Zhu and J. Xu, “Joint maneuver and beamforming design for UAV-enabled integrated sensing and communication,” *IEEE Trans. Wireless Commun.*, vol. 22, no. 4, pp. 2424-2440, Apr. 2023.
- [9] Y. Liu, S. Liu, et al., “Sensing Fairness-Based Energy Efficiency Optimization for UAV Enabled Integrated Sensing and Communication,” *IEEE Wireless Commun. Lett.*, vol. 12, no. 10, pp. 1702-1706, Oct. 2023.
- [10] O. Rezaei, M. M. Naghsh, et al., “Resource Allocation for UAV-Enabled Integrated Sensing and Communication (ISAC) via Multi-Objective Optimization,” in *IEEE ICASSP*, Rhodes Island, Greece, pp. 1-5, 2023.
- [11] J. Peng, W. Tang and H. Zhang, “Directional Antennas Modeling and Coverage Analysis of UAV-Assisted Networks,” *IEEE Wireless Commun. Lett.*, vol. 11, no. 10, pp. 2175-2179, Oct. 2022.
- [12] P. Sinha and I. Guvenc, “Impact of Antenna Pattern on TOA Based 3D UAV Localization Using a Terrestrial Sensor Network,” *IEEE Trans. Veh. Technol.*, vol. 71, no. 7, pp. 7703-7718, Jul. 2022.
- [13] L. Xiang, F. Pei, and A. Klein, “Joint Optimization of Beamforming and 3D Array Steering for Multi-antenna UAV Communications,” in *Proc. IEEE WCNC*, Dubai, United Arab Emirates, Apr. 2024.
- [14] Y. Xiong, F. Liu, et al., “On the Fundamental Tradeoff of Integrated Sensing and Communications under Gaussian Channels,” in *IEEE Trans. Inf. Theory*, vol. 69, no. 9, pp. 5723-5751, Sept. 2023.
- [15] C. B. Barneto, T. Riihonen, et al., “Beamformer Design and Optimization for Joint Communication and Full-Duplex Sensing at mm-Waves,” *IEEE Trans. Commun.*, vol. 70, no. 12, pp. 8298-8312, Dec. 2022.
- [16] C. A. Balanis, *Antenna Theory: Analysis and Design*. John Wiley & Sons, 4th ed, 2016.
- [17] S. Boyd and L. Vandenberghe, *Convex Optimization*. Cambridge University Press, 2004.
- [18] J. Bolte, S. Sabach and M. Teboulle, “Proximal alternating linearized minimization for nonconvex and nonsmooth problems,” *Mathematical Programming*, vol. 146, no. 1-2, pp. 459-494, Oct. 2014.
- [19] D. P. Palomar and Y. C. Eldar, *Convex Optimization in Signal Processing and Communications*, 2009.
- [20] J. Zhang, Y. Zhang, et al., “Robust Energy-Efficient Transmission for Wireless-Powered D2D Communication Networks,” *IEEE Trans. Veh. Technol.*, vol. 70, no. 8, pp. 7951-7965, Aug. 2021.
- [21] C. Liu and N. Boumal, *Simple algorithms for optimization on Riemannian manifolds with constraints*. Jan. 2019.
- [22] X. Li, V.-C. Andrei, et al., “Optimal Linear Precoder Design for MIMO-OFDM Integrated Sensing and Communications Based on Bayesian Cramér-Rao Bound,” arXiv:2308.12106.
- [23] P.-A. Absil, R. Mahony and R. Sepulchre, *Optimization Algorithms on Matrix Manifolds*. Princeton University Press, 2009.